

# Nondestructive Measurements of the Mechanical and Structural Properties of Nanostructured Metalattices

Begoña Abad,\* Joshua L. Knobloch, Travis D. Frazer, Jorge N. Hernández-Charpak, Hiu Y. Cheng, Alex J. Grede, Noel C. Giebink, Thomas E. Mallouk, Pratibha Mahale, Nabila N. Nova, Andrew A. Tomaschke, Virginia L. Ferguson, Vincent H. Crespi, Venkatraman Gopalan, Henry C. Kapteyn, John V. Badding, and Margaret M. Murnane



Cite This: <https://dx.doi.org/10.1021/acs.nanolett.0c00167>



Read Online

ACCESS |



Metrics & More



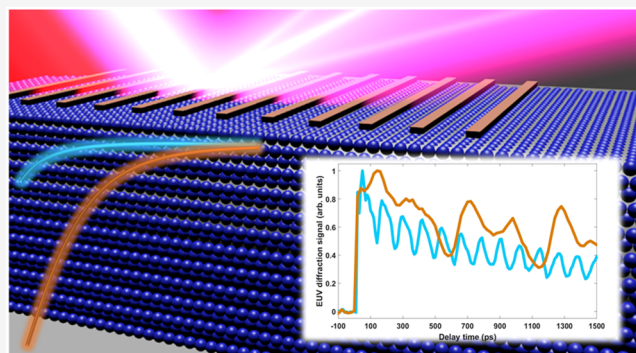
Article Recommendations



Supporting Information

**ABSTRACT:** Metalattices are artificial 3D solids, periodic on sub-100 nm length scales, that enable the functional properties of materials to be tuned. However, because of their complex structure, predicting and characterizing their properties is challenging. Here we demonstrate the first nondestructive measurements of the mechanical and structural properties of metalattices with feature sizes down to 14 nm. By monitoring the time-dependent diffraction of short wavelength light from laser-excited acoustic waves in the metalattices, we extract their acoustic dispersion, Young's modulus, filling fraction, and thicknesses. Our measurements are in excellent agreement with macroscopic predictions and potentially destructive techniques such as nanoindentation and scanning electron microscopy, with increased accuracy over larger areas. This is interesting because the transport properties of these metalattices do not obey bulk predictions. Finally, this approach is the only way to validate the filling fraction of metalattices over macroscopic areas. These combined capabilities can enable accurate synthesis of nanoenhanced materials.

**KEYWORDS:** Metalattice, Mechanical properties, Nondestructive, High harmonics, Laser, Acoustic metrology



Advances in nanofabrication have enabled the development of complex materials with intricate nanoscale structure that support dramatically different physical properties than are possible using bulk materials.<sup>1,2</sup> However, our ability to fabricate nanostructured systems has outpaced our ability to characterize their properties. For example, most current nanometrology techniques are destructive and challenging to reproduce on unique samples. Therefore, nondestructive characterization techniques that can probe large areas are critical for both enhancing our fundamental understanding of nanostructured systems and informing materials synthesis and engineering for a wide array of nanodevices.

Phononic crystals represent a very promising route for tuning the properties of next-generation nanoelectronics, thermoelectrics, and ultralight materials. These consist of periodic arrays embedded in an elastic medium, arranged in a specific lattice symmetry.<sup>3–5</sup> Nanofabrication techniques can now produce nanoscale phononic crystals with dimensions  $\ll 100$  nm (referred to as metalattices) which make it possible to engineer new elastic and transport properties.<sup>2,6</sup> To fabricate metalattices, nanospheres are first assembled into a colloidal crystal with face centered cubic (FCC) order. This base structure can be tuned from monolayer to microns in

thickness, with sphere sizes from the nanometer (nanoscale opals) to microns (opals).<sup>3,7</sup> The interstitial space between the nanospheres of the colloidal crystal is then infiltrated with another material, forming a metalattice structure for periodicities in the sub-100 nm range.

Metalattices represent an exciting class of nanostructured emerging materials, whose physical properties are not well understood. In order to tune the magnetic, elastic, or transport properties, the metalattice periodicity can be tuned to length scales comparable to the scattering or exchange lengths.<sup>2,8</sup> To understand the mechanical properties of metalattices, studies to date have focused only on one component of the metalattice—either the template or the etched-out structures, and always for periodicities  $>100$  nm. Two techniques have been used to date to extract the Young's modulus from these

**Received:** January 14, 2020

**Revised:** February 28, 2020

**Published:** March 31, 2020



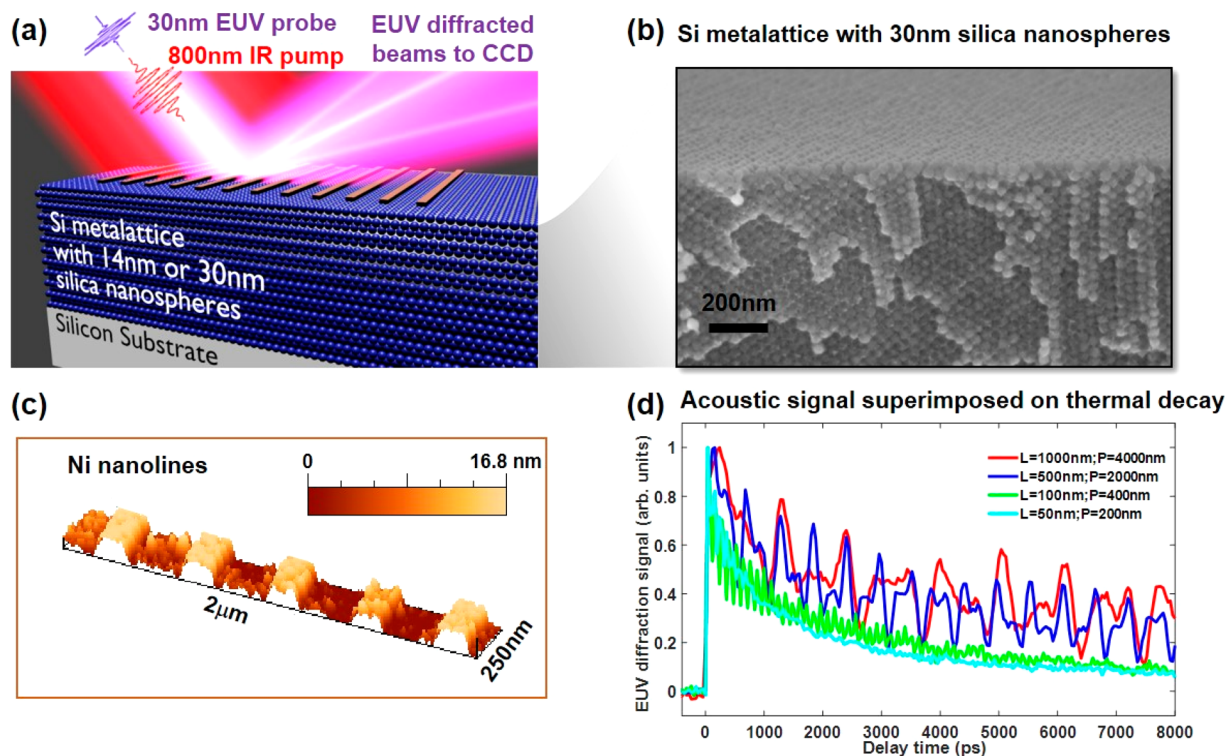


**Figure 1.** (a) EUV nanometry for extracting the thickness, Young's modulus, and filling fraction of a metalattice sample. An ultrafast laser impulsively heats a nickel grating, launching surface acoustic waves whose penetration depth is proportional to the nanoline period. The SAWs are detected by monitoring the EUV diffraction signal as a function of time delay after the laser pump pulse. (b) SEM image of a metalattice structure, fabricated from 30 nm silica nanospheres between which polycrystalline silicon is infiltrated. (c) AFM image of the  $L/P = 100$  nm/400 nm grating, where the Ni nanolines conform to the morphology of the metalattice surface. (d) EUV diffraction signal from four gratings, where the acoustic oscillations can be seen superimposed on a thermal decay.

larger templates/structures: nanoindentation and Brillouin light scattering (BLS), in combination with numerical models. For example, Still et al. used BLS in combination with numerical methods to observe a reduction in the Young's modulus compared to bulk, for silica spheres with PMMA coating, with diameters  $\sim 181$  nm.<sup>9</sup> Wang et al. utilized nanoindentation to observe an increase in the Young's modulus as the silica sphere size was reduced from 538 to 326 nm.<sup>10</sup> Nanoindentation studies of inverse opal materials, including silica coated with a titania layer,<sup>11</sup> nickel,<sup>12</sup> polysilazane,<sup>13</sup> and SiC,<sup>14</sup> exhibit enhanced mechanical properties, which are promising for the development of micron-scaled lightweight,<sup>11</sup> high-strength,<sup>12,14</sup> and crack-free<sup>13</sup> structures. These results represent extraordinary progress in the development and mechanical characterization of colloidal crystals and inverse opals with sphere sizes  $>100$  nm. However, nondestructive methods to accurately extract the mechanical and structural properties of metalattices with much smaller feature sizes, that can now be fabricated down to  $\sim 14$  nm,<sup>2</sup> are still lacking.

In this work, we demonstrate the first nondestructive measurements of the mechanical and structural properties of complex 3D nanostructured media—specifically, silicon metalattices fabricated from sphere diameters of 14 and 30 nm, with periodicities of 19 and 42 nm, respectively. This corresponds to feature sizes that are an order of magnitude smaller than have been characterized to date. We use an ultrafast laser pulse to heat a set of transducer gratings, which impulsively launch surface acoustic waves (SAWs) in the metalattice. The wavelength of the SAW can be tuned by varying the transducer

grating periodicity, which also changes the SAW penetration depth into the metalattice and the silicon substrate. We then monitor the SAW frequency from the time-dependent change in extreme ultraviolet (EUV) light diffracted off the grating. This allows us to simultaneously extract the acoustic dispersion, as well as the Young's modulus, thickness, and filling fraction of the metalattice. The extracted mechanical and structural properties agree well with macroscopic predictions and with other experimental measurements when possible. This is interesting because the transport properties of the same metalattices do not agree with bulk models. The measured metalattice thicknesses agree with scanning electron microscopy (SEM) images, while the extracted Young's modulus is in agreement with nanoindentation measurements and also achieves higher accuracy. Finally, this technique represents the only approach to date to nondestructively validate the filling fraction of deep-nanoscale metalattices. It also has advantages over destructive electron imaging because it can probe over large areas and does not suffer from material contrast issues. These results can enable precise fabrication, characterization, and understanding of materials with tailored mechanical and transport properties.

## RESULTS

**Metalattices.** Our samples consist of two metalattices that are fabricated by infiltrating silicon into arrays of either 14 or 30 nm diameter silica nanospheres, that are slightly overlapped after a sintering process (see Figure 1b). The face centered cubic metalattice structures have periodicities of 19 and 42 nm, respectively, and filling fractions of 76%. The metalattices are

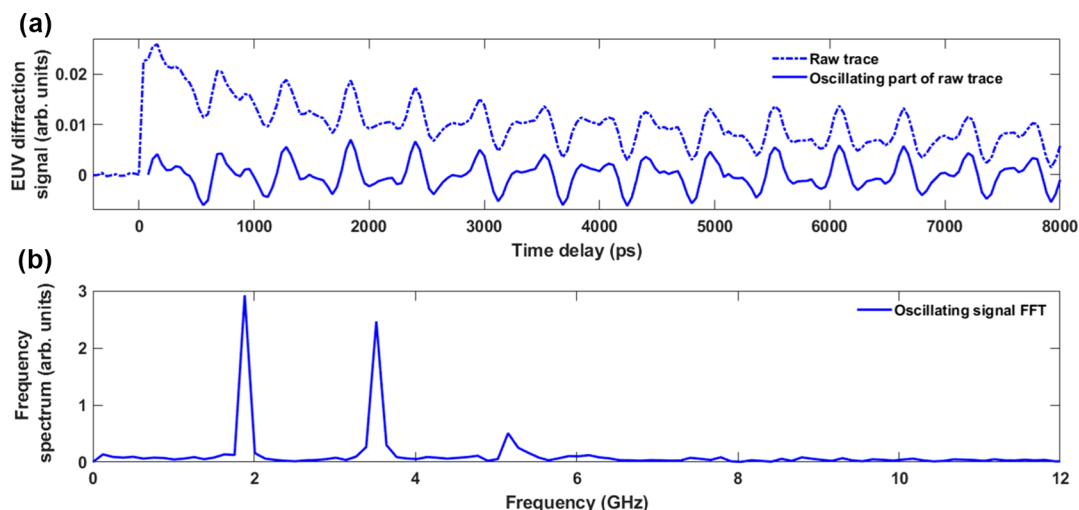


**Figure 2.** Surface acoustic wave analysis. (a) Change in EUV diffraction from a grating of line width 500 nm and period 2000 nm as a function of time delay after laser excitation. The dashed line corresponds to the total signal, while the solid line only includes the oscillating part after removing the thermal decay by the matrix pencil method. (b) Frequency spectrum calculated from the Fourier transform of the oscillating part of the signal. The fundamental frequency together with second and third harmonics are clearly resolved.

fabricated via high pressure confined chemical vapor deposition to deposit amorphous silicon into the interstitial voids of the silica templates (see the [Supporting Information](#) for more details). This infiltration forms an intricate network where more capacious regions, called meta-atoms, with sizes below 5 nm are connected by thin necks, known as meta-bonds, which are as thin as 2 nm. The samples studied here consist of  $\sim 30$  layers of spheres.

**Acoustic Characterization.** To launch surface acoustic waves (SAWs) with adjustable penetration depths, a set of transducer gratings with different periodicities are fabricated on top of the metalattices by e-beam lithography, which conform the surface of the metalattice, as shown in [Figure 1c](#). These transducers can be impulsively heated by an ultrafast 0.8  $\mu\text{m}$ , 30 fs laser pulse. The resultant high frequency (GHz) surface acoustic waves have a penetration depth of approximately  $1/\pi$  of their wavelength (set by the grating period).<sup>15,16</sup> Therefore, a SAW can be fully confined to the metalattice for sufficiently small grating periods.<sup>17,18</sup> To span the first Brillouin zone of the metalattice acoustic dispersion, a total of five nickel gratings with different line widths,  $L = 1000, 500, 100, 100,$  and  $50$  nm, and periods,  $P = 4000, 2000, 800, 400,$  and  $200$  nm, respectively, are deposited on the sample surface.

The SAW frequency is extracted by monitoring the change in diffraction efficiency of an ultrafast EUV high harmonic probe beam as a function of delay time between the laser pump and EUV probe pulses, as represented in [Figure 1a](#). The EUV probe beam is generated via high harmonic upconversion of the femtosecond laser beam in argon, to create  $\sim 5$  harmonics that span a wavelength range of  $\sim 25\text{--}33$  nm, and with a pulse duration of  $\sim 10$  fs.<sup>19</sup> Even for these complex metalattices, with grating transducers on top of multilayered nanostructures, EUV nanometrology achieves an extraordinary signal-to-noise ratio: [Figure 1d](#) shows the raw EUV diffraction traces for four different gratings. The initial sharp rise in the EUV diffraction signal is given by the rapid expansion of the nanolines, where the typical deflection that is being measured is on the order of  $\sim \text{pm}$ . This is followed by SAW oscillations whose frequencies vary according to the SAW wavelength (i.e., period of the

grating). Finally, a slow thermal decay can also be seen in the raw data, that occurs as heat is dissipated from the transducers into the metalattice.

**Acoustic Dispersion Relation.** To extract the acoustic wave dispersion, we analyze the SAW frequencies after subtracting the slow thermal decay component (see [Figure 1d](#)). [Figure 2a](#) shows the change in diffraction as a function of pump–probe time delay from a grating of period of 2000 nm and line width of 500 nm, where both the total EUV diffraction signal and the extracted oscillating component are plotted. Because we launch the acoustic waves with a square wave grating, several higher harmonics are also generated in addition to the fundamental SAW, which produce multifrequency oscillations in the signal. A Fourier analysis of the oscillating part of the signal gives the SAW fundamental and harmonic frequencies launched for a given grating, as shown in [Figure 2b](#). We further analyze SAW frequencies by using the chirp- $Z$ <sup>20</sup> transform and matrix pencil method<sup>21</sup> to extract thorough values for each grating, resolving frequencies as high as 60 GHz. For the range of acoustic wavelengths and frequencies explored here, all of the excited frequencies are below the predicted phononic bandgap for these periodic structures, which depends on the period and speed of sound and is estimated to be  $\sim 180$  and  $\sim 80$  GHz for the 14 and 30 nm metalattices, respectively.<sup>6</sup>

To properly interpret our measured frequencies, we must account for the finite thickness of the metalattice layer. [Figure 3a](#) shows the measured SAW velocity (calculated from the measured SAW frequency and the grating period) versus penetration depth, normalized by the thickness of the metalattice, as measured by cross-sectional scanning electron microscopy (SEM). Parts b and c of [Figure 3](#) show two cross-sectional SEM images corresponding to gratings with line width/period of 500 nm/2000 nm ([Figure 3b](#)) and 100 nm/400 nm ([Figure 3c](#)), where the SAWs are drawn as a guide. Parts d and e of [Figure 3](#) also illustrate the penetration depth at which the energy of the acoustic wave has dropped by  $1/e$ . From [Figure 3a](#), it is clear that, for shorter wavelength SAWs that correspond to smaller grating periods and penetration depths, the SAW velocity measured is that of the metalattice

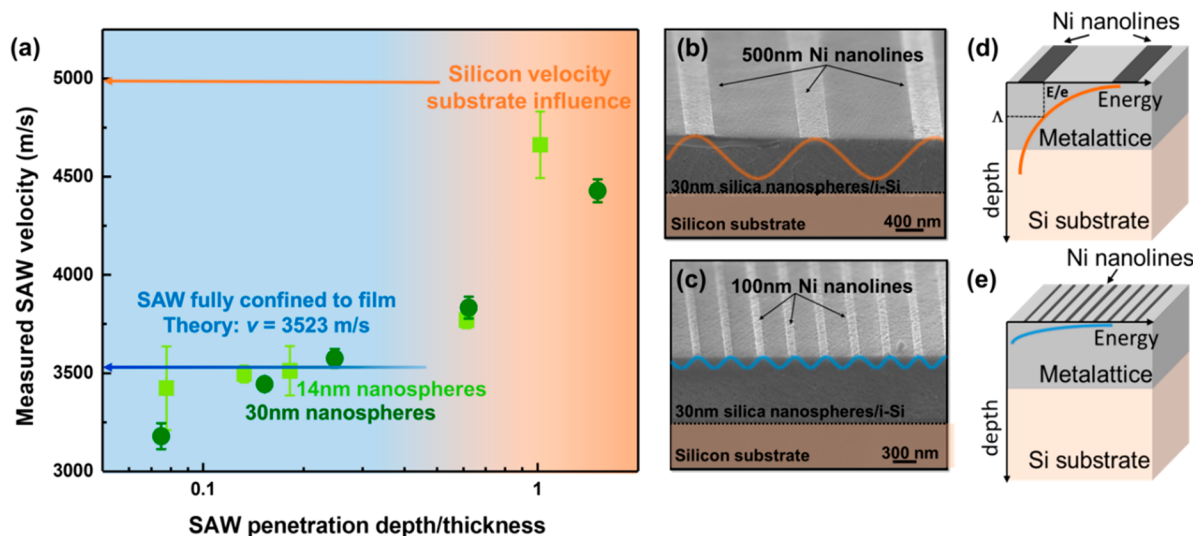


**Figure 3.** (a) Surface acoustic wave dispersion of the metalattices, showing the SAW velocity as a function of penetration depth, normalized by the metalattice layer thickness. Each point corresponds to the fundamental SAW launched by each grating on the 30 nm (circles) and 14 nm template (squares) metalattices. Both metalattices have the same filling fraction and thus are predicted to have the same SAW velocity. At large penetration depths, the SAW velocity approaches that of the silicon substrate ( $\sim 5000$  m/s), as expected. For smaller penetration depths, the measured metalattice velocities agree with macroscopic predictions (blue line). At the smallest penetration depths, deviations from theory are observed and not surprising, as only a few metalattice layers at the surface are probed. (b, c) Cross-sectional SEM images of the 30 nm metalattice for two different gratings with line width/period 500 nm/2000 nm and 100 nm/400 nm and thicknesses of 1045 and 855 nm, respectively. The dashed line depicts the boundary between the silicon substrate and the metalattice. The penetration depths of the acoustic waves are drawn in both images. The penetration depth corresponds to the depth at which the acoustic wave energy has dropped by  $1/e$ , shown schematically for (d) large grating (long penetration depth) and (e) small grating (short penetration depth). The SAW velocities associated with these two samples correspond to the second and fourth circles from the left in part a.

layer (3523 m/s). This value is in agreement with that calculated from finite element analysis (FEA), assuming an ideal FCC silica/silicon structure with a filling fraction of 76% (see the [Supporting Information](#) for more details). In the case of the smallest grating on the 30 nm metalattice, the 50 nm line width with 200 nm spacing grating, the SAW penetration depth of  $\sim 60$  nm is probing only over one to two nanosphere layers which may not probe the average mechanical properties of this metalattice. For the longer wavelength SAWs, with sufficiently deep penetration so that  $\sim 20$ – $50\%$  of the SAW is propagating in the silicon substrate, the measured velocity is much higher, close to that of silicon,  $\sim 5000$  m/s.<sup>22</sup>

In [Figure 3a](#), we see that both the 14 and 30 nm Si infiltrated metalattices have the same measured SAW velocities, which is interesting, since both have the same filling fraction and nano-order; i.e., they are scaled versions of each other. In this case, we can conclude that the SAW velocity only depends on the percentage of silica/silicon in each sample and that there are no size effects observed even for these deep nanoscale regimes. These values also agree with the elastic properties extracted from an FEA continuum mechanics model where the fraction and structure of each metalattice sample is included, and the interfaces are assumed to be perfect. This shows that EUV nanometrology can extract the dispersion relation of nanostructured materials and also that these silicon metalattices were fabricated with extraordinary high quality.

**Mechanical and Structural Properties.** Since we now know that the mechanical properties of these metalattices follow continuum mechanics, we can model the transducer/metalattice/silicon substrate multilayer structure to predict the SAW propagation. When compared with the experimentally measured SAW frequencies/velocities, this can be used to extract the Young's modulus and also the metalattice

thicknesses. In general, the velocity of the propagating acoustic waves has an analytical relation to the elastic properties; however, the nanograting on the surface of the metalattice alters the SAW velocity. To account for this, we utilize FEA to replicate the dynamics of the experiment and fit the elastic properties of the metalattice film.<sup>15,16</sup> We model the metalattice as a uniform film of effective elastic properties on a silicon substrate, with a Ni nanograting on the surface of the film. Using FEA, we compute the eigenmodes of this structure and calculate the SAW-likeness coefficient defined by Nardi et al., which quantifies how localized the energy is to the surface, to locate the frequency of the mode observed in the experiment.<sup>15,16</sup>

We first extract the Young's modulus for the metalattice film by fitting the simulations to the experiment for grating sizes where the SAW is fully confined to the metalattice. As seen in [Figure 4a](#), we find excellent agreement between the extracted Young's modulus and the calculated value from continuum FEA models, at 92 GPa (see the [Supporting Information](#)) for 100 nm/400 nm and 100 nm/800 nm line width/period gratings. In order to confirm the values extracted using EUV nanometrology, we also performed nanoindentation experiments on the same metalattices (see the [Supporting Information](#) for experimental details). These measurements gave values of the Young's moduli of 83 and 85 GPa for the 14 and 30 nm metalattices, respectively. These values reconfirm that both metalattice films have the same properties. Most importantly, the average Young's modulus value from nanoindentation agrees well with that extracted from EUV measurements, taking into account the larger  $\sim 10\%$  error associated with nanoindentation (see the [Supporting Information](#)). For both techniques, Poisson's ratio was assumed to be the same as the one obtained from continuum FEA models, at

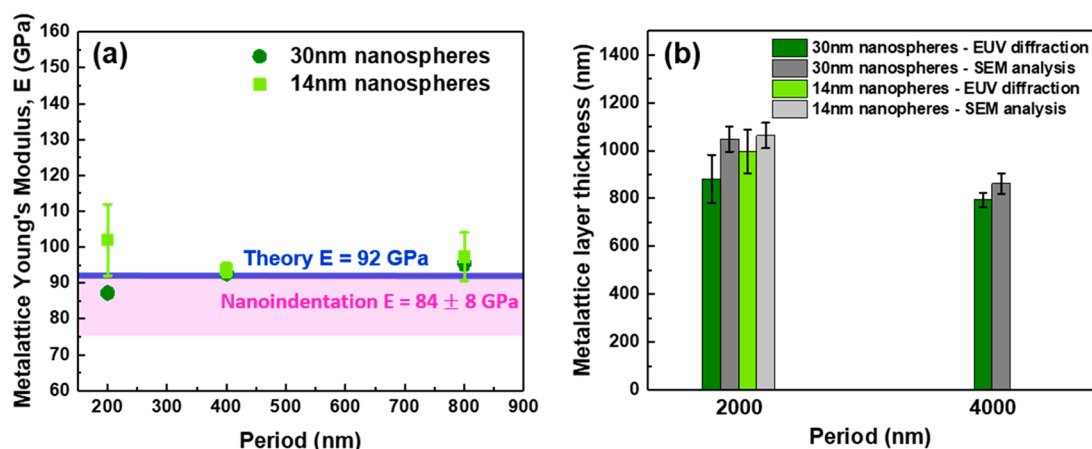


**Figure 4.** Young's modulus and thickness as a function of grating period, where the latter sets the SAW wavelength ( $P$ ) and penetration depth ( $P/\pi$ ). (a) For small periods, SAW are fully confined within the metalattice—we therefore extract the intrinsic Young's modulus of the metalattice without any substrate contribution. This agrees well with both continuum mechanics calculations and nanoindentation. (b) For large grating periods, where the SAW are partially confined and influenced by the substrate, we use the intrinsic Young's modulus to nondestructively extract the thickness of the metalattice, which is in agreement with the values obtained from SEM images.

0.18. This is a good approximation, since the constituent materials have similar Poisson's ratios (0.22 and 0.17 for silicon<sup>23</sup> and silica,<sup>24</sup> respectively).

Knowing the Young's modulus of the metalattice, we can now use this value in the same multilayer model to nondestructively extract the thickness of the metalattice layer. Here we fit the simulations to SAW data from the large grating sizes, where the SAWs penetrate into the Si substrate. We then find the thickness of the metalattice layer that reproduces the observed SAW frequency (Figure 4b). In order to corroborate the thicknesses extracted by this procedure, we also acquired cross-sectional SEM images for each of the gratings. Figure 4b shows that there is good agreement between the metalattice thicknesses measured by SEM and those extracted from EUV nanometrology for the two metalattices: the deviation between both methods was between 5 and 15%. This is partly due to transverse variation in the metalattice thicknesses. In general, EUV nanometrology makes it possible to extract the materials properties over a much larger area ( $\sim 100 \mu\text{m} \times 100 \mu\text{m}$  square) compared with SEM image analysis ( $\sim 1 \text{ nm} \times 10 \mu\text{m}$  square).

Finally, it is also worth noting that our multilayer model predictions also depend on the filling fraction of silica to silicon within the metalattice structure, e.g., metalattice density varies depending on whether the silica spheres are overlapping or touching, which is given by the nanofabrication conditions. From both sets of simulations of the data (multilayer model and continuum mechanics model), we can extract a best-fit value of 76% for the filling fraction. The agreement between theory and multiple measurements of the Young's modulus and thickness confirms this filling fraction value (see the Supporting Information for more details). Note that this value is challenging to experimentally confirm using other approaches such as TEM, which measures the thickness of the necks—from which the filling fraction can be extracted.

Our EUV technique can be applied to any isotropic complex nanomaterial and extract information that is not possible using other techniques. From our current results, it is clear that this technique can probe different morphologies, as we show for the case of two metalattices that are the scaled version of each other. In addition, in ref 17, our SAW-based technique was

able to probe ultrathin isotropic films in a very reliable manner, including how the Young's modulus and Poisson's ratio evolve as a function of hydrogenation. This information cannot be extracted from other techniques. Therefore, this technique is able to probe 2D systems like thin films<sup>17</sup> and, in this work, we extend it to 3D nanostructured systems. Because this is the first demonstration on a 3D nanostructured material, this is why we compared with nanoindentation and simulation to establish the error bars. Moreover, these complex materials cannot be probed by other methods such as impulsive stimulated thermal scattering (ISTS), also known as the transient grating technique. In ISTS, absorbing materials can be characterized by crossing two visible laser beams at the surface of the sample,<sup>25–27</sup> thereby creating a sinusoidal excitation pattern that launches acoustic waves. However, for the metalattices studied here that are made of silicon and silica, the optical absorption properties are nonuniform; thus, an intricate heating profile made of a convolution between a sinusoidal pattern and the silicon geometry would be created. In addition, the diffraction limit of visible light makes it extremely challenging to achieve sufficiently small periods to confine the SAWs within the metalattices, which is key to decoupling the elastic properties from the metalattice thickness.

## CONCLUSIONS

Our results demonstrate that EUV nanometrology is a powerful nondestructive technique to probe mechanical and structural properties of extremely complex nanostructures that would not be possible otherwise. We use it to extract the Young's moduli, thicknesses, and filling fractions of two nanoscale 3D silicon metalattices. To our knowledge, this is the only approach that can accurately characterize the properties of metalattices over macroscopic sample areas. In addition, they show that the mechanical properties of these metalattices follow macroscopic predictions, in contrast to their spin and energy transport properties, which dramatically change at such small feature sizes. This study shows that metalattices at these scales can be designed with tunable mechanical properties and transport properties.

## ■ ASSOCIATED CONTENT

### Supporting Information

The Supporting Information is available free of charge at <https://pubs.acs.org/doi/10.1021/acs.nanolett.0c00167>.

Further information about the metalattice fabrication and details on the data analysis, acoustic simulations, and nanoindentation experiments (PDF)

## ■ AUTHOR INFORMATION

### Corresponding Author

**Begoña Abad** – Department of Physics, JILA and STROBE NSF Science & Technology Center, University of Colorado and NIST, Boulder, Colorado 80309, United States; [orcid.org/0000-0001-7589-7973](https://orcid.org/0000-0001-7589-7973); Email: [b.abad@jila.colorado.edu](mailto:b.abad@jila.colorado.edu)

### Authors

**Joshua L. Knobloch** – Department of Physics, JILA and STROBE NSF Science & Technology Center, University of Colorado and NIST, Boulder, Colorado 80309, United States

**Travis D. Frazer** – Department of Physics, JILA and STROBE NSF Science & Technology Center, University of Colorado and NIST, Boulder, Colorado 80309, United States; [orcid.org/0000-0002-5162-4230](https://orcid.org/0000-0002-5162-4230)

**Jorge N. Hernández-Charpak** – Department of Physics, JILA and STROBE NSF Science & Technology Center, University of Colorado and NIST, Boulder, Colorado 80309, United States; [orcid.org/0000-0003-3296-6929](https://orcid.org/0000-0003-3296-6929)

**Hui Y. Cheng** – Department of Chemistry, Biochemistry and Materials Research Institute, Pennsylvania State University, University Park, Pennsylvania 16802, United States

**Alex J. Grede** – Department of Chemistry, Biochemistry and Materials Research Institute, Pennsylvania State University, University Park, Pennsylvania 16802, United States

**Noel C. Giebink** – Department of Chemistry, Biochemistry and Materials Research Institute, Pennsylvania State University, University Park, Pennsylvania 16802, United States; [orcid.org/0000-0002-3798-5830](https://orcid.org/0000-0002-3798-5830)

**Thomas E. Mallouk** – Department of Chemistry, Biochemistry and Materials Research Institute, Pennsylvania State University, University Park, Pennsylvania 16802, United States; [orcid.org/0000-0003-4599-4208](https://orcid.org/0000-0003-4599-4208)

**Pratibha Mahale** – Department of Chemistry, Biochemistry and Materials Research Institute, Pennsylvania State University, University Park, Pennsylvania 16802, United States

**Nabila N. Nova** – Department of Chemistry, Biochemistry and Materials Research Institute, Pennsylvania State University, University Park, Pennsylvania 16802, United States

**Andrew A. Tomaschke** – Mechanical Engineering, University of Colorado, Boulder, Colorado 80309, United States

**Virginia L. Ferguson** – Mechanical Engineering, University of Colorado, Boulder, Colorado 80309, United States

**Vincent H. Crespi** – Department of Chemistry, Biochemistry and Materials Research Institute, Pennsylvania State University, University Park, Pennsylvania 16802, United States

**Venkatraman Gopalan** – Department of Chemistry, Biochemistry and Materials Research Institute, Pennsylvania State University, University Park, Pennsylvania 16802, United States; [orcid.org/0000-0001-6866-3677](https://orcid.org/0000-0001-6866-3677)

**Henry C. Kapteyn** – Department of Physics, JILA and STROBE NSF Science & Technology Center, University of Colorado and NIST, Boulder, Colorado 80309, United States

**John V. Badding** – Department of Chemistry, Biochemistry and Materials Research Institute, Pennsylvania State University, University Park, Pennsylvania 16802, United States

**Margaret M. Murnane** – Department of Physics, JILA and STROBE NSF Science & Technology Center, University of Colorado and NIST, Boulder, Colorado 80309, United States

Complete contact information is available at: <https://pubs.acs.org/10.1021/acs.nanolett.0c00167>

### Author Contributions

M.M.M., J.V.B., and H.C.K. conceived the experiment. B.A., J.L.K., and T.D.F. performed the acoustic measurements and analyzed the data. B.A. and J.L.K. performed the acoustic simulations. B.A. and J.L.K. performed AFM experiments. A.A.T., V.L.F., and B.A. performed nanoindentation experiments. P.M. and H.Y.C. fabricated the metalattices. A.J.G. fabricated the nanolines. N.N.N. took the SEM images. All authors discussed the results and either wrote or reviewed the paper.

### Notes

The authors declare no competing financial interest.

## ■ ACKNOWLEDGMENTS

The authors gratefully acknowledge support from the STROBE National Science Foundation Science & Technology Center, Grant No. DMR-1548924, for the setups and methods, and the Penn State Center for Nanoscale Science, an NSF-sponsored Materials Science and Engineering Center under award DMR-1420620, for synthesizing the samples. The authors also acknowledge nanoindenter funding from the NSF Major Research Instrumentation Award No. 1338154: “MRI Acquisition: An integrated platform for combined multi-scale mechanical and chemical analysis to inform functional materials design”. J.L.K. acknowledges support from an SRC Fellowship. H.C.K. is partially employed by KMLabs.

## ■ REFERENCES

- (1) Han, J. E.; Crespi, V. H. Abrupt Topological Transitions in the Hysteresis Curves of Ferromagnetic Metalattices. *Phys. Rev. Lett.* **2002**, *89* (5), 197203.
- (2) Liu, Y.; Kempinger, S.; He, R.; Day, T. D.; Moradifar, P.; Yu, S. Y.; Russell, J. L.; Torres, V. M.; Xu, P.; Mallouk, T. E.; Mohny, S. E.; Alem, N.; Samarth, N.; Badding, J. V. Confined Chemical Fluid Deposition of Ferromagnetic Metalattices. *Nano Lett.* **2018**, *18* (1), 546–552.
- (3) Armstrong, E.; O’Dwyer, C. Artificial Opal Photonic Crystals and Inverse Opal Structures-Fundamentals and Applications from Optics to Energy Storage. *J. Mater. Chem. C* **2015**, *3* (24), 6109–6143.
- (4) Barako, M. T.; Sood, A.; Zhang, C.; Wang, J.; Kodama, T.; Asheghi, M.; Zheng, X.; Braun, P. V.; Goodson, K. E. Quasi-Ballistic Electronic Thermal Conduction in Metal Inverse Opals. *Nano Lett.* **2016**, *16* (4), 2754–2761.
- (5) Liontas, R.; Greer, J. R. 3D Nano-Architected Metallic Glass: Size Effect Suppresses Catastrophic Failure. *Acta Mater.* **2017**, *133*, 393–407.
- (6) Maldovan, M. Sound and Heat Revolutions in Phononics. *Nature* **2013**, *503* (7475), 209–217.
- (7) Vogel, N.; Retsch, M.; Fustin, C.-A.; del Campo, A.; Jonas, U. Advances in Colloidal Assembly: The Design of Structure and Hierarchy in Two and Three Dimensions. *Chem. Rev.* **2015**, *115* (13), 6265–6311.
- (8) Han, J. E.; Crespi, V. H. Tuning Fermi-Surface Properties through Quantum Confinement in Metallic Metalattices: New Metals from Old Atoms. *Phys. Rev. Lett.* **2001**, *86* (4), 696.

- (9) Still, T.; Sainidou, R.; Retsch, M.; Jonas, U.; Spahn, P.; Hellmann, G. P.; Fytas, G. The “Music” of Core-Shell Spheres and Hollow Capsules: Influence of the Architecture on the Mechanical Properties at the Nanoscale. *Nano Lett.* **2008**, *8* (10), 3194–3199.
- (10) Wang, Y.; Dou, S.; Shang, L.; Zhang, P.; Yan, X.; Zhang, K.; Zhao, J.; Li, Y. Effects of Microsphere Size on the Mechanical Properties of Photonic Crystals. *Crystals* **2018**, *8* (12), 453.
- (11) do Rosário, J. J.; Lilleodden, E. T.; Waleczek, M.; Kubrin, R.; Petrov, A. Y.; Dyachenko, P. N.; Sabisch, J. E. C.; Nielsch, K.; Huber, N.; Eich, M.; Schneider, G. A. Self-Assembled Ultra High Strength, Ultra Stiff Mechanical Metamaterials Based on Inverse Opals. *Adv. Eng. Mater.* **2015**, *17* (10), 1420–1424.
- (12) Pikul, J. H.; Özering, S.; Liu, B.; Zhang, R.; Braun, P. V.; Deshpande, V. S.; King, W. P. High Strength Metallic Wood from Nanostructured Nickel Inverse Opal Materials. *Sci. Rep.* **2019**, *9* (1), 719.
- (13) Zhang, Z.; Shen, W.; Ye, C.; Luo, Y.; Li, S.; Li, M.; Xu, C.; Song, Y. Large-Area, Crack-Free Polysilazane-Based Photonic Crystals. *J. Mater. Chem.* **2012**, *22* (12), 5300–5303.
- (14) Zhou, J.; Li, H.; Ye, L.; Liu, J.; Wang, J.; Zhao, T.; Jiang, L.; Song, Y. Facile Fabrication of Tough SiC Inverse Opal Photonic Crystals. *J. Phys. Chem. C* **2010**, *114* (50), 22303–22308.
- (15) Nardi, D.; Banfi, F.; Giannetti, C.; Revaz, B.; Ferrini, G.; Parmigiani, F. Pseudosurface Acoustic Waves in Hypersonic Surface Phononic Crystals. *Phys. Rev. B: Condens. Matter Mater. Phys.* **2009**, *80* (10), 104119.
- (16) Nardi, D.; Travagliati, M.; Siemens, M. E.; Li, Q.; Murnane, M. M.; Kapteyn, H. C.; Ferrini, G.; Parmigiani, F.; Banfi, F. Probing Thermomechanics at the Nanoscale: Impulsively Excited Pseudosurface Acoustic Waves in Hypersonic Phononic Crystals. *Nano Lett.* **2011**, *11* (10), 4126–4133.
- (17) Hernandez-Charpak, J. N.; Hoogeboom-Pot, K. M.; Li, Q.; Frazer, T. D.; Knobloch, J. L.; Tripp, M.; King, S. W.; Anderson, E. H.; Chao, W.; Murnane, M. M.; Kapteyn, H. C.; Nardi, D. Full Characterization of the Mechanical Properties of 11–50 Nm Ultrathin Films: Influence of Network Connectivity on the Poisson’s Ratio. *Nano Lett.* **2017**, *17* (4), 2178–2183.
- (18) Li, Q.; Hoogeboom-Pot, K.; Nardi, D.; Murnane, M. M.; Kapteyn, H. C.; Siemens, M. E.; Anderson, E. H.; Hellwig, O.; Dobisz, E.; Gurney, B.; Yang, R.; Nelson, K. A. Generation and Control of Ultrashort-Wavelength Two-Dimensional Surface Acoustic Waves at Nanoscale Interfaces. *Phys. Rev. B: Condens. Matter Mater. Phys.* **2012**, *85* (19), 195431.
- (19) Rundquist, A.; Chang, Z.; Herne, C.; Backus, S.; Murnane, M. M.; Kapteyn, H. C. Phase-Matched Generation of Coherent Soft X-Rays. *Science (Washington, DC, U. S.)* **1998**, *280* (5368), 1412–1415.
- (20) Bluestein, L.I. A linear filtering approach to the computation of discrete Fourier transform. *IEEE Trans. Audio Electroacoust.* **1970**, *18* (4), 451–455.
- (21) Hoogeboom-Pot, K. M.; Turgut, E.; Hernandez-Charpak, J. N.; Shaw, J. M.; Kapteyn, H. C.; Murnane, M. M.; Nardi, D. Nondestructive Measurement of the Evolution of Layer-Specific Mechanical Properties in Sub-10 Nm Bilayer Films. *Nano Lett.* **2016**, *16* (8), 4773–4778.
- (22) Auld, B. A. *Acoustic Fields and Waves in Solids*, Vol. II; Wiley: New York, 1973.
- (23) Hopcroft, M. A.; Nix, W. D.; Kenny, T. W. What Is the Young’s. *J. Microelectromech. Syst.* **2010**, *19* (2), 229–238.
- (24) Bansal, N. P.; Doremus, R. H. *Handbook of Glass Properties*; Academic Press: Orlando, FL, 1986.
- (25) Rogers, J. A.; Maznev, A. A.; Banet, M. J.; Nelson, K. A. Optical generation and characterization of acoustic waves in thin films. Fundamentals and Applications. *Annu. Rev. Mater. Sci.* **2000**, *30*, 117–57.
- (26) Banet, M. J.; Fuchs, M.; Rogers, J. A.; Rienold, J. H., Jr.; Knecht, J. M.; Rothschild, M.; Logan, R.; Maznev, A. A.; Nelson, K. A. High-precision film thickness determination using a laser-based ultrasonic technique. *Appl. Phys. Lett.* **1998**, *73*, 169–171.
- (27) Rogers, J. A.; Fuchs, M.; Banet, M. J.; Hanselman, J. B.; Logan, R.; Nelson, K. A. Optical system for rapid materials characterization with the transient grating technique: application to nondestructive evaluation of thin films used in microelectronics. *Appl. Phys. Lett.* **1997**, *71*, 225–227.